Report on Schellenberger ice core activities

1. Introduction

Here we report the activities done after the ice core drilling in the Schellenberger Eishöhle in July 2016, and the following measurements done in Eurocold Lab in Milano. These activities were founded by the Verein für Höhlenkunde Schellenberg, University of Bochum and University of Milano-Bicocca (Itay).

Cave deposits, together with peat bogs, swamps lakes and tree rings, represent an important archive of past climatic and environmental information for continental areas, and proper archives from medium to low altitude mountains, like cave sediments and speleothems, can be found well below the limit of the glaciers (**Turri et al., 2003; Haeberli and Alean, 1985**). The underground ice deposits, in function of their nature and process of formation, can contain elements that allow the study of past interactions with the climatic and environmental history of a region (**Turri et al., 2003, Luetscher, 2005; Citterio et al., 2004; Kern et al., 2011; May et al., 2011, Persoiu and Pazdur, 2011)**.

Even if the underground ice deposits are usually well-protected archives (**Perroux, 2001**), there are different problems in studying ice caves with respect to the surface glaciers. Frequently, hypogean ice deposits are found in direct connection with the epigean environment (i.e. collapse doline) (**Persoiu and Pazdur, 2011**), but some of that are located deeper in the caves without any direct connection to the surface (**Turri et al., 2003**). Therefore, mechanisms of ice formation and growth are not necessarily the same as in the surface glacier deposit. To have a better knowledge of this precious archive, both “near-surface” epigean and hypogean environments should be studied in detail, because understanding the interactions of these two environments allows the

interpretation of the surrounding environment and climate (also in the past). **Ford and Williams (1989)** described seven types of hypogean ice deposits that are described in the literature and he classified them in to two main groups; “exogenous” and “endogenous” ice deposits. Exogenous ice is normally snow deposit, which enters directly into a cave and after some times it transforms into ice (or firn). Because of the direct contact with the external environment, a large amount of organic materials can drop in the cave and accumulate within the ice deposit. Endogenous ice can be produced by many sources like, ice flow, stalactites, stalagmites, ice film, frozen ponds (or lakes), ice from sublimation, ice in sediment clasts, all mainly from external water from melting snow or rain percolating into the cave, with few or absent organic material.

Schellenberger Eishöhle is a big alpine cave (total length: 3621 m, total depth: - 260 m), including a static ice cave part which has been run as a show cave since 1925. Apart from the 500m long ice cave part, there is one major non-ice part, which forks off close to the entrance in a northeasterly direction and leads through several deep shafts to the deepest point of the cave (- 260 m). The cave is situated at 1570m asl at the foot of the Eastern walls of Untersberg (the cave entrance is marked in Fig. 1). The access to the cave is by a 4m high and 20m wide portal, which leads to Josef-Ritter-von-Angermayer-Halle, the largest room in the cave with a length of 70m and a width of 40 m, that is illuminated by daylight. The floor of this hall, 17m below the entrance level, completely consists of a major ice monolith, which is surrounded by the cave trail. The two passages Wasserstelle and Mörkdom connect to the deepest part of the ice cave called Fuggerhalle, 41m below entrance level. They are also partly covered with ice.

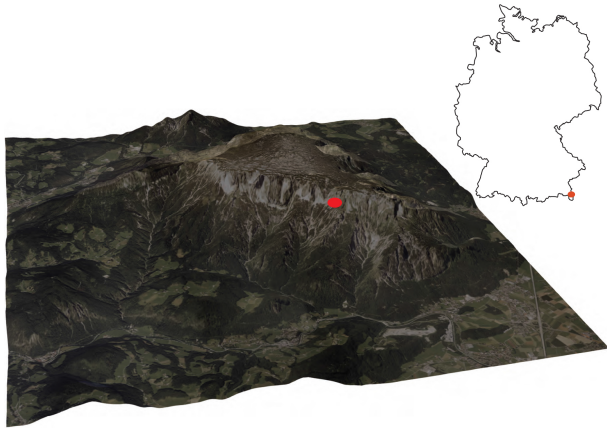

Figure 1. Location of Schellenberger Eishöhle at the foot of the east face of Untersberg. The mountain is viewed from the East, the length of the edges is 11 km (orthophotos: ©2003/2004, Salzburg AG and DI Wenger-Oehn, digital elevation model: Bundesamt für Eich- und Vermessungswesen in Wien). The map inlay shows the location of Untersberg in Germany.

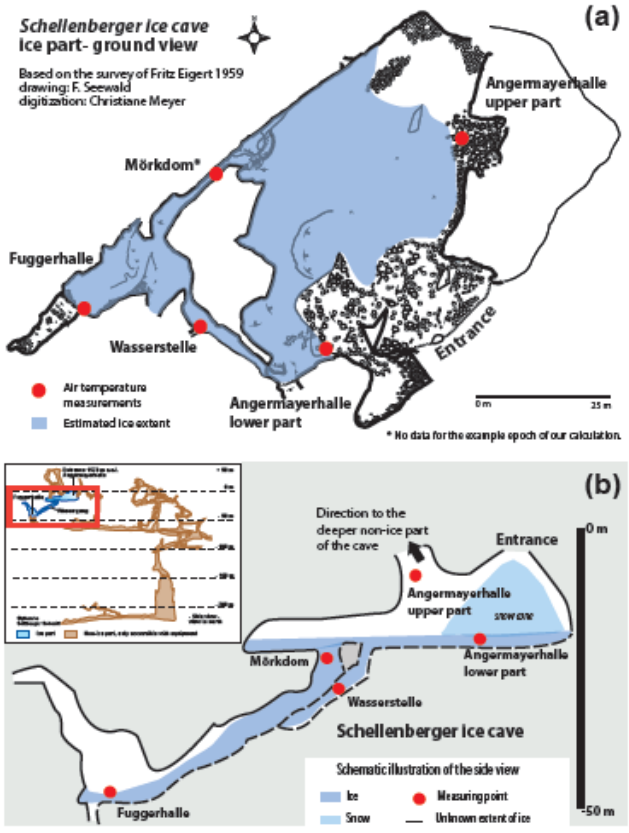

Figure 2. Ground map and side view of Schellenberger Eishöhle. Red cross is the position of the ice core drilling

2. **Methods**

A 800 cm ice core was drilled in the spring 2016 in Angermayerhalle ice deposit, close to the main entrance of the Schellemberger ice cave (fig. 2), by lightweight drilling system recovery max 80 cm length and 10 cm diameter. The drilling activities was done in the position where the radar survey (Colucci & Forte personal communications) define the maximum depth of the Angermayerhalle ice deposit (around 10 m), at more than 5 m far from the tourist paths. Each ice core was measured and packed in plastic bags for preservation and stored in insulated boxes with dry ice for the conservation during the transport to the cold rooms of EuroCold Lab at University of Milano-Bicocca (Milan, Italy).

In the cold lab the entire ice core was logged for the visual stratigraphy using a digital camera and 1 cm slice along the vertical axis was cut for thin sections. One quarter of the ice cores was used for chemical sampling at 10 cm resolution, collected in plastic bottles, and maintained frozen till the measurements was done.

Cations and anions were measured using the Ion Chromatography (Thermo Scientific^{TM} Dionex^{TM}, Waltham, MA, USA). During the chemical measurements the ¼ of ice core were cut each 10 cm and pH, conductivity, K, Mg, Ca, Na, NH4, N03 and SO4 where done 3 time each sample for have more statistical significance of the measures. Table 1 and Fig 3 show the results of the measurements done.

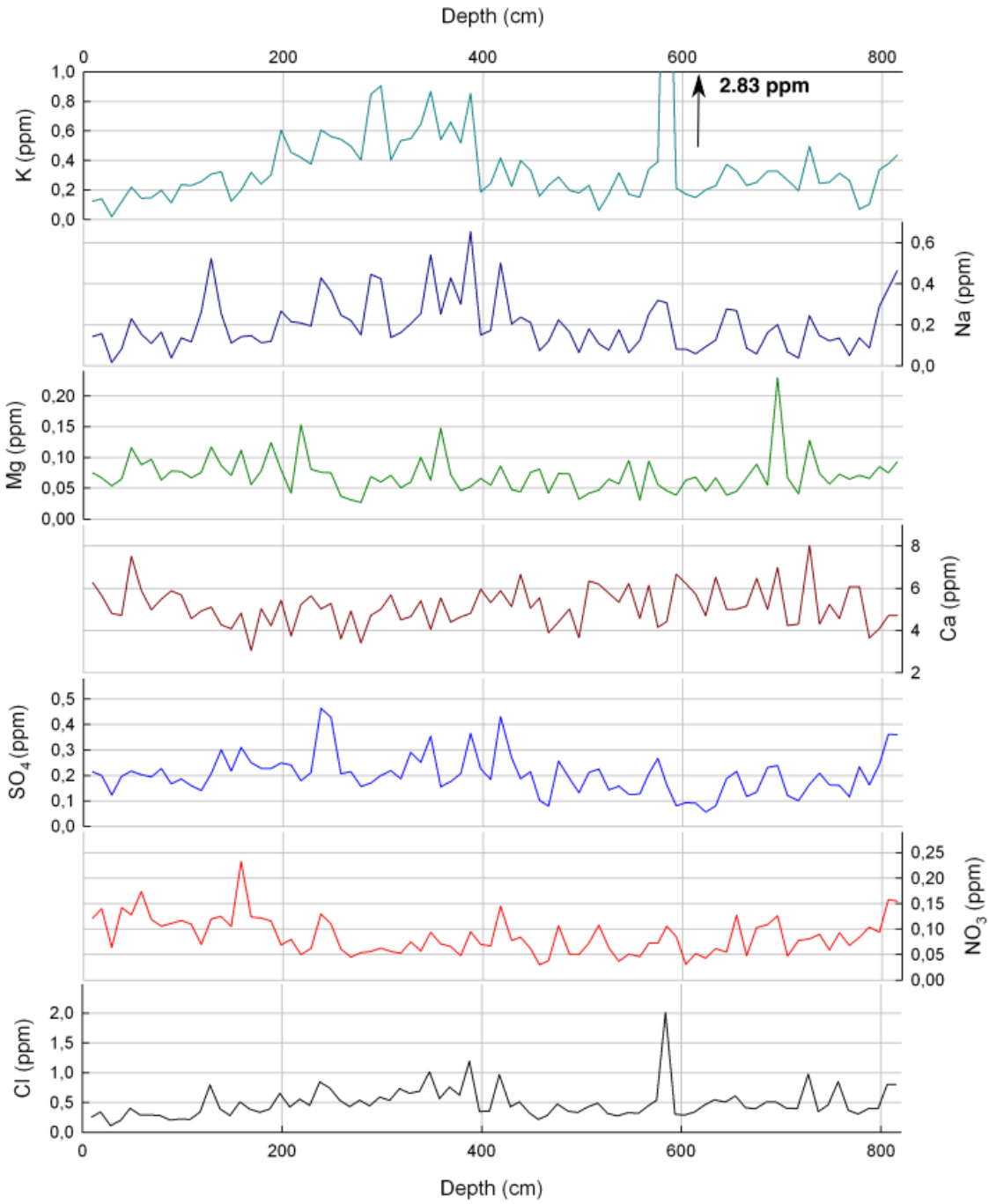

Fig. 3 - Main chemical stratigraphy from the Schellenberger ice core

Sulphate ion has mainly three sources: marine (sea-salt spray and biological process), anthropogenic sources and volcanic eruptions. Of the latter, the most spectacular and anomalous signals are related to explosive volcanic eruptions that can spew millions of tons of sulphate into

the atmosphere and have low (days to months) atmospheric residence time. In order to differentiate the sulphate signal related to volcanic eruption from that of the marine-derived, the total sulphate concentration is normalised using sodium (Na^+) as marine reference species, and using the sulphate-to-sodium ratio (0.252) in sea water:

$$\text{(no-sea-salt sulphate) } (nss{SO_4}^{2-}) = ({SO_4}^{2-}) - 0.252\ (Na^+). \qquad (1)$$

It is well established that Na^+ is the most reliable marker for sea salt compared to Cl^- (**Thamban *et al.*, 2006**).

A specimen of leave, find at 799 cm depth (fig. 4), was sampled for radiocarbon date, prepared in University of Milano-Bicocca and dated by AMS accelerator at the CNR of Caserta (Italy). The resulting date was not reliable for the ice core dating because too young. In effect the results in radiocarbon age is 100+/- 50 years BP, that means, using the OXCAL© Radiocarbon Calibration Software from the University of Oxford (UK) a calendar age from 1940 to 1650 AD, to large time span for any possibility of age interpretation.

Fig. 4: The leave at 799 cm depth, used for radiocarbon dating

Thin sections imaging did visual stratigraphy of the ice core. Each slide, 9x9 cm and oriented, are thinned till 1 mm thickness and observed by universal stage cross-polarized filters (Rigsby, 1951; Langway, 1958). A reconstruction of the possible ice facies was done for evaluates the possible ice accumulation phases and understand the existing hiatus on the stratigraphy. The entire ice core was explored for define the bubble orientation, clear ice areas, presence of dust layers or lens, and presence of organic materials, also for the radiocarbon dates. For each thin section a digital picture was take using the transmission light stage using single and cross polaroid filters, each image was recorded digitally on the Universal Stage for well understand the variability in the crystal fabric, bubble distribution and size, and presence of exotic materials (dust, organics, stones, etc…).

3. Discussion and results

3.1 Ice Core Stratigraphy

The ice core stratigraphy derived by thin section permit to evaluate how the ice deposit will be accumulated or eroded by the atmosphere and cave dynamic. There is mainly 2 different type of crystals related to the mechanism of deposition.

a) Columnar ice is large ice crystals, normally vertically elongated, with a clear continuously C-Axis orientation related to the water pond freezing during the winter season or cold periods, These crystal grow very slowly after the freezing of the water surface. The closure of the surface permit crystal growing only vertically in the water. Because the process is very slow, the ceystal grow using the same optical orientation, that permit in thin section to observe similar colours with very few crystal boundaries. Typical ice crystals of all the frozen lakes, frozen ponds and sea ice, in ice caves can be related to the melting of snow from the main entrance, dripping water or effect of the cave management.

b) Hexagonal/rounded ice normally are related to medium to small crystals, less than 1 cm diameter, with rounded shape, sometimes with angular boundaries, but not easily to observe without lens or microscope. The large difference in C-Axis orientation, permit to have a very granular area, with more scattered optical colours. These crystals are normally related to the snow metamorphism after snowfalls or avalanches reaching the main hall. Direct snowfalls, wind blowing snow or falling of snow deposits from the mountain wall above the main entrance can provide large amount of snow on the ice deposit and the following cold/warm cycles (day/night or seasonal) reduce the large snow crystals in rounded grains that ca have the same shape of the pure ice (Hexagonal system) or, more general, rounded grains. Snow after that transformation were named FIRN. The reducing of the crystal volume permit at the firn to reduce the volume of

the entire layer (packing) and consequently reduce the porosity. The following melting processes, normally during the summer season, fill the voids by water and create a more compact ice, create also water and air bubbles.

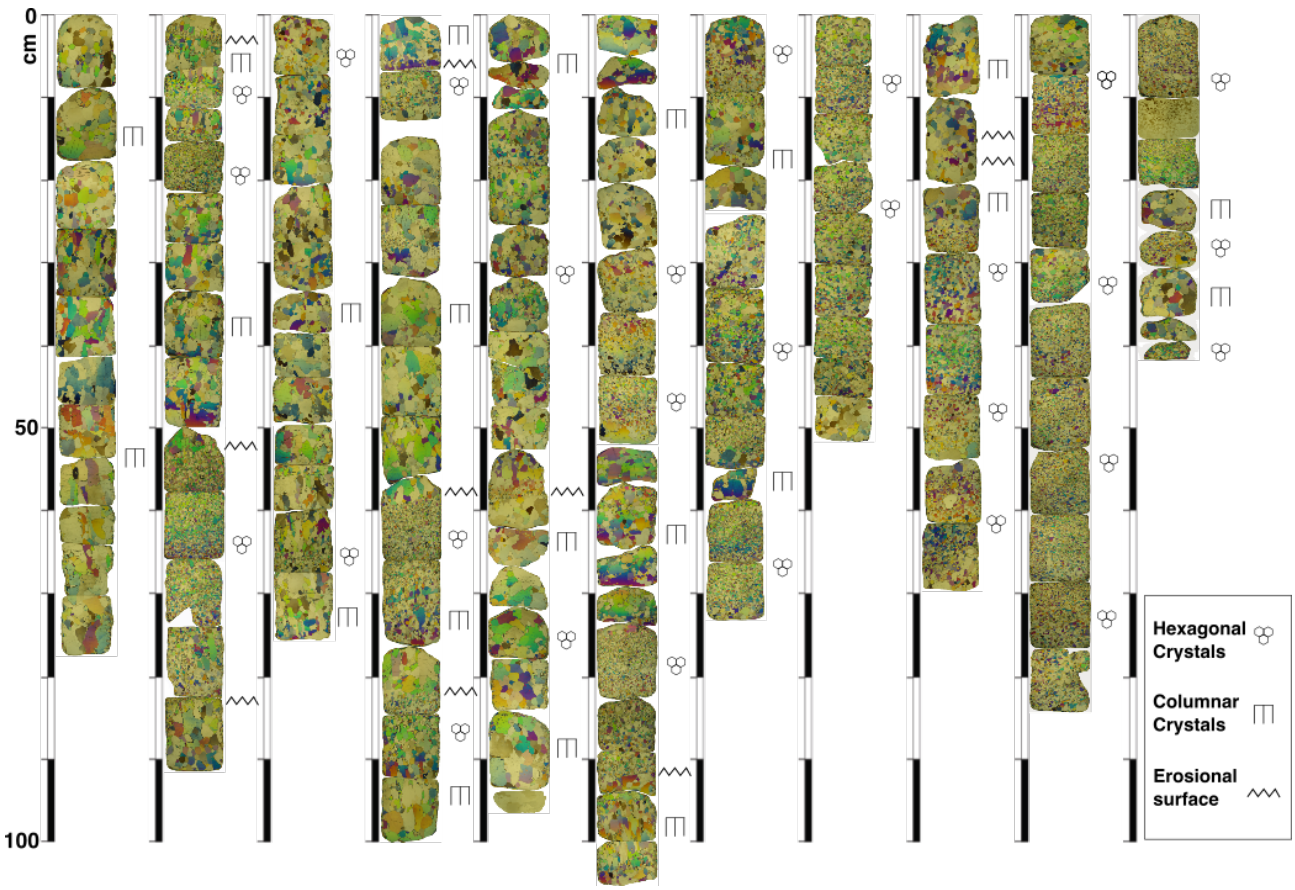

Fig. 5 – Schellenberger ice core visual stratigraphy.

The entire stratigraphy present alternates of different ice fabrics mainly dominated by one of other type of crystals (fig. 5). There is some layering, related to this alternance, but is not possible to evaluate any regular changes in these layers, nor any seasonality as expected by the strong differences between the winter and summer accumulation behaviour. The lack in seasonality can be relate to two main reasons. The first is that the annual climatic cycle do not permit to have a regular alternance of the different accumulation mechanisms. During the winter the level of the snow at the entrance can change significantly with differences in the snow accumulation.

Moreover, avalanches and strong snowfalls can seal the entrance for long periods or permit the blowing snow to enter in deep of the main hall. At the same time the summer season can be more wet, or drier as well as the mean seasonal temperature change significantly along the years. Do not forget also the tourism impact of on the micrometeorology of the ice cave.

The figure 6 show the entire stratigraphy of the ice core, and the original of the pictures can be download in the Google Drive folder (ask Valter Maggi for the Access).

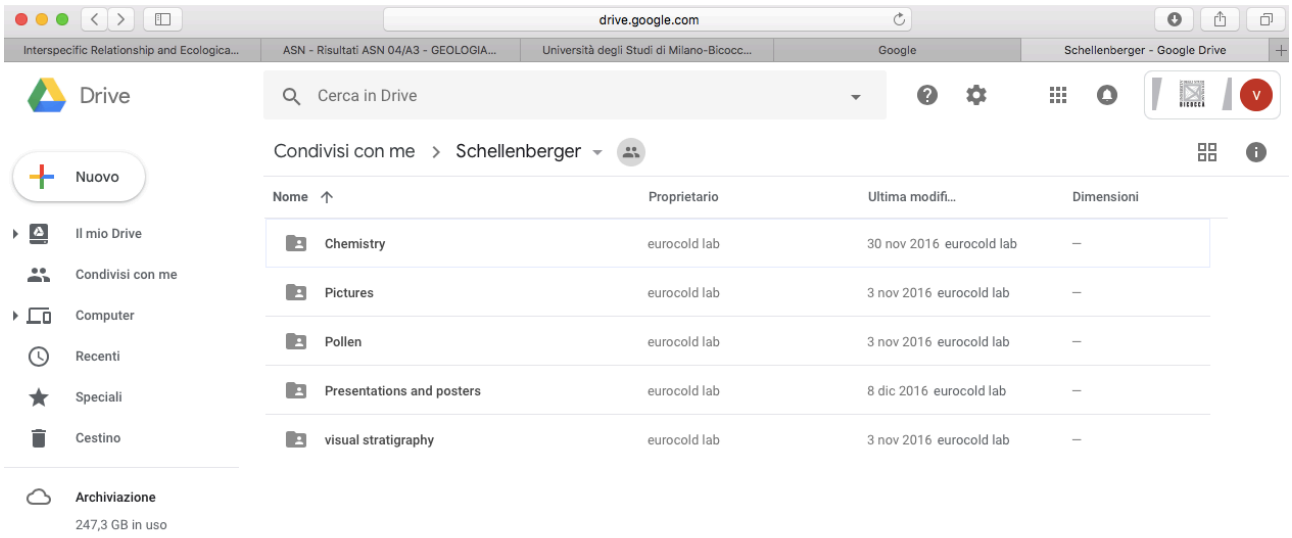

Fig. 6 – Schellenberger ice core database on Google Drive.

3.2 No-sea salt-Sulfates and volcanic signials

Despite the general scattering of data and the low correlation coefficient (r=0,197), the application of a cubic correlation fit to the nss-sulphate from Schellemberger ice core provide a clear trend showing a relative maximum of nss-sulfate between 600 and 700 cm depth reaching the men value of 0,18 mg/l, and relative minimum between 200 and 300 cm depth, reaching a mean value

of 0.11 mg/l. As demonstrate by the low correlation coefficient, the variability of the nss-sulfate is very large, with spikes below 0.05 mg/l and above the 0.35 mg/l (fig 7). The residuals analyses of the cubic correlation show that all samples are included in the 2 of variability (96 % of confidence), except for three outliers at 410, 572 and 582 cm depth, that represent the two main spikes off all the record (respectively 0.305, and 0,337-0.356 mg/l) (fig. 6).

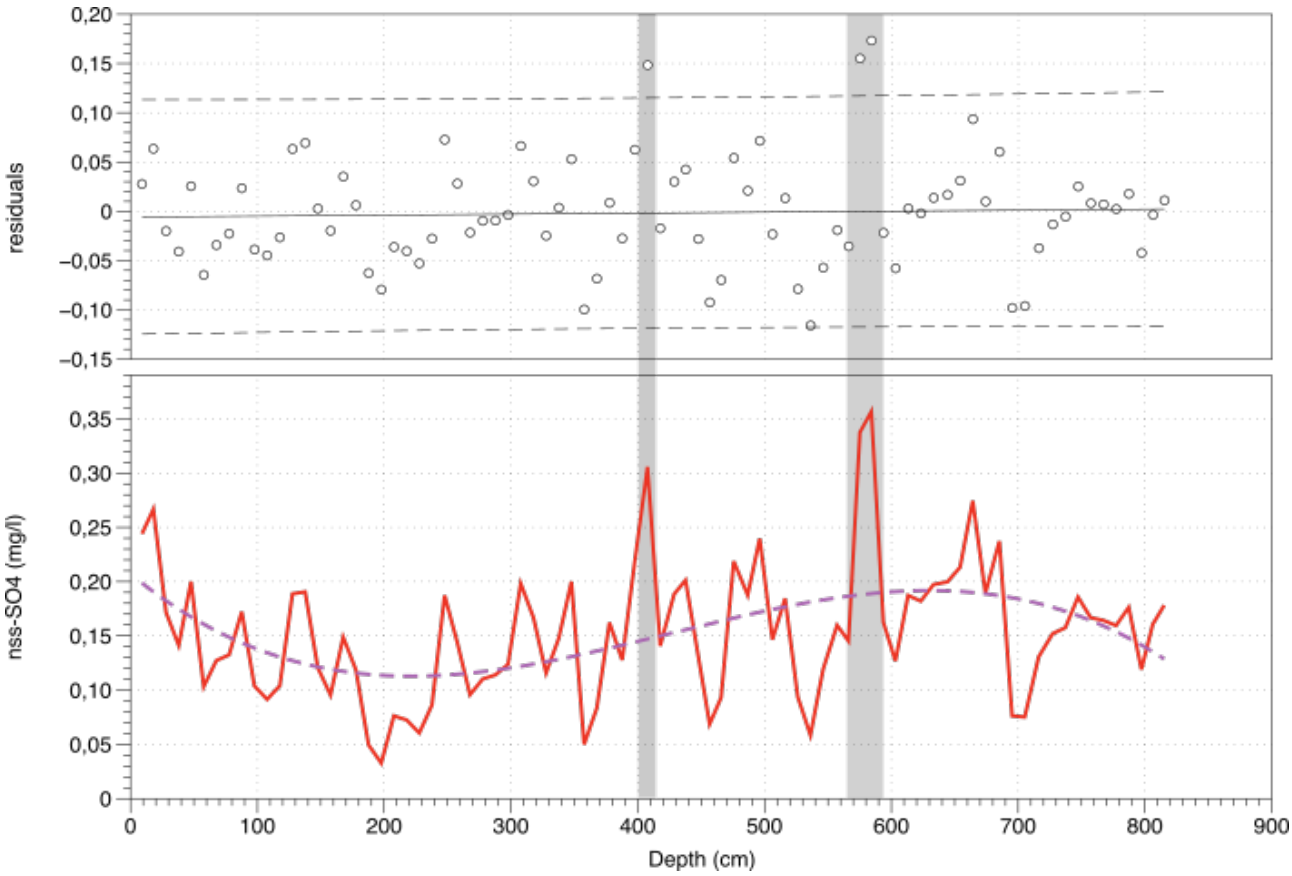

Fig. 7: Lower panel, record of nss-Sulfates with the cubic correlation curve (r2=0,299). The upper panel show the residuals of the correlation with the confidence lines of 96% (dashed lines). The gray areas represent the two peaks related to the outliers in the correlation, related to the possible volcanic events.

Because the radiocarbon date of the ice core bottom is “modern age” so will be probably less than 1950 AD, a tentative of correlation of the nss-sulfate ice core trend were compared with a global sulphate emission dataset, mainly related to the atmospheric human impact and explosive

volcanic events (Smith et al., 2011). In effect the general emission trend from the late 60ties till the 2005 (Smith et al, 2011) show a trend similar to the nss-sulfate. In fact, the emission trends show a continuous increase from the 1850 to the end of 70ies beginning of 80ties when reach the maximum emission (more than 130000 Gt of SO_2), and then a decrease related to the improving of the energy production efficiency. This decrease stops at the beginning of the new millennium (minimum less than 110000 Gt of SO_2) because the increase of the emerging economies as China and India (Smith et al., 2011) (Fig. 7).

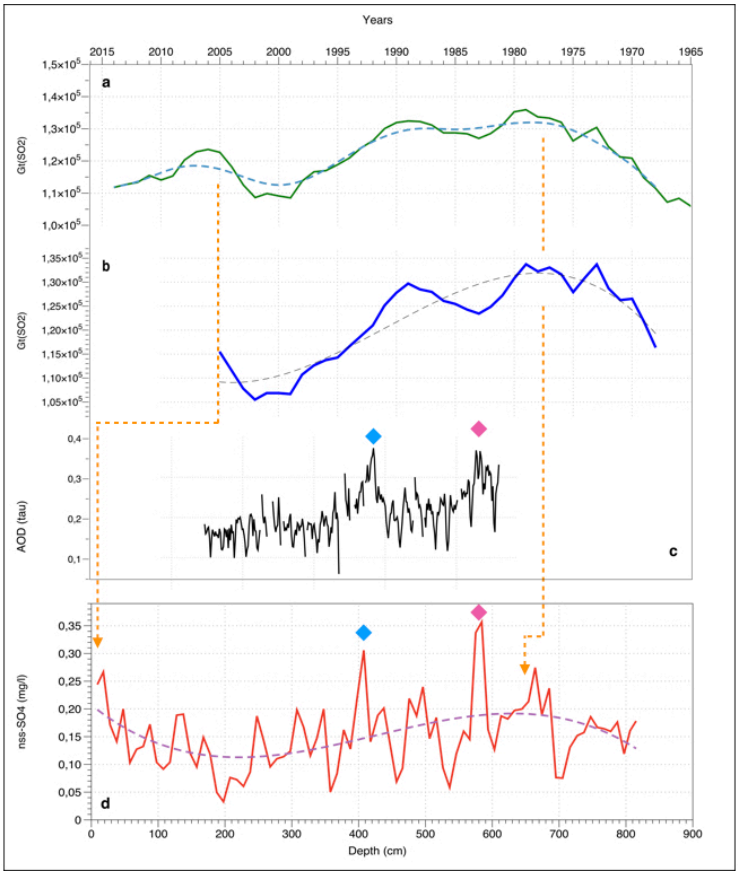

Fig. 8: Comparison between the Sulphur Dioxide Emission dataset (a and b), the (c) Aerosol Optical Depth (AOD), and the nss-Sulfate from SIC (d). The emission data and blue line Smith et al., 2011) are smoothed using a Loess correlation method (blue and grey dashed lines). The AOD, is the mean NASA-GACP model for Europe/Mediterranean area (-15 to 40 E and 15 to 50N gridded data, Tegen et al., 1997) The nss-Sulfate record (red line) are smoothed using a cubic correlation (purple dashed line) with r2=0.195. The gray areas represent the possible nss-sulfate peaks from possible volcanic eruption (Pinatubo 1991 add El Chichon 1983), used for synchronizing the two records. The arrows present the possible correlation between the relative minimum (1-year shift) and relative maximum (4 years shift) between the two correlation lines.

A simply overlapping of the two records does not permit a clear synchronization between the two dataset. Despite the emission data is annual spaced, the ice core record (nss-sulfate and all others) does not present a continuous accumulation (different snowfalls, avalanches, dripping water) and is not possible to exclude that part of the stratigraphy are not melting away. For this reason for the synchronization need some reference horizons well known in both the records. The comparison of the two records could be enhanced using the two nss-sulfate peaks represented by the three outliers, as reference horizon of possible volcanic spikes.

In the last 50 years there are hundreds of volcanic eruptions around the world, but if we limit the search at VEI (Volcanic Explosive Index) = 4, that represent by Plinian eruptions with more the 10km of tropospheric plume, and definite stratospheric injection of the materials (Newhall and Self, 1982), the number is reduced to few events, especially if related to the northern Hemisphere transport.

From continuous Lidar measurements done in Garmisch-Partenkirchen (Germany) from 1976, the European stratosphere are affect mainly by 2 huge impact: the El Chichon in the 1982, and the Pinatubo in the 1991. The Lidar measurements at 694.3 nm wavelength, representing the integrated stratospheric backscatter coefficient, show that the duration of the El Chichon and Pinatubo eruptions are not similar in term of southern German stratospheric composition. The El Chichon present an increase of the Lidar signal reaching the maximum after 200 days of the eruption and preserve the signal for more than 5 years before reaching the background value; the Pinatubo present a more rapid increase of the atmospheric sulfates reaching the maximum after 100 days from the eruption, and decrease at background levels in the next 5 years (Trickl et al., 2013; Jager, 2005).

El Chichon is a Mexican volcano (17.360 N, 93.228 W) that in the 1982 erupted 3 times the 29 of March, the 4 of April and the 27 of May (all with VEI 5), killing more than 1900 people (mainly during the 29 march eruption) (source: NGDC-NOAA Significant Volcanic Eruption Database https://www.ngdc.noaa.gov/hazard/volcano.shtml) and inject on the atmosphere of 7 million metric tonnes of solfur dioxide (SO2) and 20 million metric tonnes of particulate material into the stratosphere (Rebock, 2002). A net cooling effect of approximately 0.3°C was estimated as a result of the El Chichón aerosol (Angell and Korshover, 1983; Handler, 1989), but the overall potential cooling caused by the El Chichón cloud was moderated by warming associated with El Niño-Southern Oscillation (Angell, 1988, 1990).

Pinatubo is a Philippian volcano (15.130 N; 120.350 E) erupted the 15 June 1991 (VEI 6), killing more than 450 people, eject in atmosphere around 17 million of metric tonnes of solfur dioxide (SO2). Pinatubo had a much larger radiative influence than El Chichón in the Southern Hemisphere (Dutton and Christy, 1992). Pinatubo's cloud caused about 1.7 times the global radiative forcing of El Chichón, making the estimated cooling of 0.5°C.

Comparing the sulphate emission record and the SIC nss-sulfate record, is possible to adjust the two correlation curves overlapping the relative maximum and the relative minimum, is possible to observe that the two outlier spikes drop between 1982-1983 for the 560-580 cm depth spike and between 1990 and 1991 for the 410 cm depth spike. These good correlations between the correlation curves and the ages of the two volcanic spikes permit to create a preliminary depth-age relationship for the SIC enough reliable for calculate the accumulation rate of the upper 8 m of ice deposit.

Observing the nss-sulfate record, the two volcanic spikes present different thickness, with the El Chichon related to 2 samples covering more than 20 cm of ice record, instead of the Pinatubo only 1 sample representative of 10 cm of record. These differences are not very representative but is in

the direction of the real events happen in the European atmosphere with the El Chichon eruption more persistent of the Pinatubo, despite the differences in the VEI index.

3.5 Preliminary age-depth relationship

The mean annual accumulation rate (MAAR) was estimate using the two volcanic peaks of El Chichon (1983) and Pinatubo (1991), using the following relationship:

$$\lambda = \frac{\Delta depth}{\Delta age} \quad [cm_{ieq}\ year^{-1}] \qquad \text{eq. 1}$$

where is the accumulation age in cm of ice equivalent per year, *depth* is the difference in depth between the two volcanic events, and *age* is the difference in age between the two volcanic events (Tab. 1). The result is 17.77 that represent 16,29 cm of water equivalent using the maximum density of ice (0.917 g cm^{-3}) (Patterson, 2004). This equation permit to estimate the minimum water equivalent MAAR, because the ice density used is the maximum possible, normally related to pure ice (without any bubbles or impurities).

Using the MAAR in ice equivalent obtained by volcanic spikes differences, is possible to extrapolate to the surface and to the bottom the depth/age relationship. The 410 cm of ice from the surface to the Pinatubo volcanic spike is an age of 19.4 years reaching the year 2014 instead of 2016 the age of the drilling. Using the same relationship till the bottom of ice core, at 820 cm depth, the depth is 2 that represent 11 years, with a bottom age of 1968 (+/- 1 years) calendar years.

The lack between the drilling year and the year extrapolated by the MAAR between the two volcanic markers, can be related to 1) melting of part of the ice deposit during the last summer

seasons, or 2) decrease of the MAAR in the last 25 years. As show in the visual stratigraphy the presence of melting surfaces in the top 400 cm that can influence the accumulation rate, reducing (or cancel) the annual layers. In other hand, is difficult to consider that the MAAR is constant along all the last 50 years. If the surface represents the 2016, the *age* from the Pinatubo marker is 25 years and using the top 410 cm as *depth* the is 16.40 (15.0 cm w.e.) and will be used as the lower limit of the Schellenberger ice core MAAR.

Bibliography

Newhall, Christopher G.; Self, Stephen (1982). "The Volcanic Explosivity Index (VEI): An Estimate of Explosive Magnitude for Historical Volcanism"(PDF). *Journal of Geophysical Research*. **87** (C2): 1231–1238.

Langway CC Jr (1958) Ice fabrics and the universal stage. *SIPRE Tech. Rep.* 62

Rigsby GP (1951) Crystal fabric studies on Emmons Glacier, Mount Rainier, Washington. *J. Geol.*, 59(6), 590–598

Smith, SJ, J van Aardenne, Z Klimont, RJ Andres, A Volke, and S Delgado Arias. (2011). Anthropogenic Sulfur Dioxide Emissions: 1850–2005, Atmospheric Chemistry and Physics, 11:1101–1116.

Tegen, I., P. Hollrig, M. Chin, I. Fung, D. Jacob, and J. Penner, 1997: Contribution of different aerosol species to the global aerosol extinction optical thickness: Estimates from model results. *J. Geophys. Res.*, **102**, 23895-23915, doi:10.1029/97JD01864.

Trickl, T., Giehl, H., Jäger, H., and Vogelmann, H.: 35 yr of stratospheric aerosol measurements at Garmisch-Partenkirchen: from Fuego to Eyjafjallajökull, and beyond, Atmos. Chem. Phys., 13, 5205-5225, doi:10.5194/acp-13-5205-2013, 2013.

Jager H., 2005. Long-term record of lidar observations of the stratospheric aerosol layer at Garmisch-Partenkirchen. J. Geophis. Res. VOL. 110, D08106, doi:10.1029/2004JD005506

Table 1

	Sample	Cl mg/l	NO3 mg/l	SO4 mg/l	Ca mg/l	Mg mg/l	Na mg/l	K mg/l
1	9 cm 1	0,253	0,122	0,214	6,266	0,075	0,143	0,125
2	9 cm 1	0,344	0,140	0,200	5,653	0,067	0,157	0,140
3	10 cm 1	0,113	0,064	0,123	4,807	0,054	0,016	0,019
4	10 cm 2	0,197	0,142	0,197	4,724	0,065	0,083	0,121
5	3,5 cm 1	0,402	0,128	0,217	7,516	0,116	0,230	0,219
6	10 cm 2	0,288	0,174	0,203	5,904	0,088	0,155	0,144
7	10 cm 2	0,292	0,119	0,194	4,979	0,097	0,109	0,147
8	6,5 cm 2	0,281	0,106	0,227	5,490	0,063	0,165	0,198
9	10 cm 3	0,205	0,111	0,167	5,880	0,078	0,038	0,113
10	10 cm 3	0,223	0,117	0,186	5,682	0,077	0,136	0,236
11	10 cm 3	0,215	0,110	0,160	4,562	0,067	0,117	0,230
12	10 cm 3	0,340	0,070	0,141	4,926	0,076	0,263	0,257
13	6,5 cm 3	0,792	0,120	0,207	5,110	0,117	0,523	0,308
14	10 cm 4	0,393	0,125	0,301	4,269	0,087	0,255	0,323
15	10 cm 4	0,280	0,105	0,217	4,082	0,071	0,111	0,123
16	10 cm 4	0,510	0,233	0,310	4,833	0,112	0,142	0,199
17	5 cm 4	0,387	0,124	0,250	3,053	0,056	0,147	0,319
18	10 cm 5	0,334	0,122	0,228	5,034	0,078	0,113	0,240
19	10 cm 5	0,392	0,116	0,227	4,226	0,124	0,119	0,302
20	10 cm 5	0,654	0,069	0,249	5,437	0,080	0,268	0,606
21	10 cm 5	0,423	0,080	0,241	3,737	0,042	0,215	0,454
22	3 cm 5	0,555	0,050	0,179	5,235	0,153	0,209	0,420
23	10 cm 6	0,451	0,062	0,211	5,640	0,081	0,194	0,375
24	7 cm 6	0,846	0,130	0,464	5,026	0,076	0,429	0,607
25	10 cm 7	0,742	0,110	0,428	5,278	0,075	0,362	0,562
26	10 cm 7	0,539	0,061	0,207	3,607	0,037	0,247	0,543
27	7,5 cm 7	0,429	0,045	0,215	4,927	0,031	0,221	0,496
28	10 cm 8	0,538	0,054	0,157	3,415	0,027	0,151	0,403
29	10 cm 8	0,442	0,056	0,170	4,718	0,069	0,446	0,847
30	10 cm 8	0,591	0,063	0,200	5,014	0,060	0,425	0,906
31	10 cm 8	0,535	0,056	0,219	5,684	0,071	0,138	0,401
32	10 cm 8	0,731	0,053	0,187	4,510	0,051	0,162	0,534
33	3 cm 8	0,654	0,075	0,291	4,656	0,060	0,205	0,547
34	10 cm 9	0,687	0,057	0,251	5,412	0,100	0,254	0,646
35	10 cm 9	1,016	0,094	0,354	4,052	0,063	0,541	0,867
36	10 cm 9	0,564	0,071	0,156	5,545	0,147	0,252	0,541
37	10 cm 9	0,760	0,066	0,176	4,400	0,072	0,429	0,659
38	5 cm 9	0,623	0,048	0,207	4,648	0,046	0,301	0,519
39	10 cm 10	1,193	0,095	0,365	4,810	0,053	0,655	0,854
40	10 cm 10	0,350	0,070	0,226	5,958	0,066	0,150	0,187
41	10 cm 10	0,354	0,067	0,184	5,321	0,055	0,173	0,244

42	5 cm 10	0,965	0,145	0,431	5,887	0,086	0,501	0,416
43	11 cm 11	0,428	0,078	0,270	5,132	0,048	0,204	0,225
44	9 cm 11	0,511	0,084	0,187	6,661	0,044	0,237	0,398
45	10 cm 11	0,327	0,062	0,215	5,058	0,076	0,211	0,334
46	9 cm 11	0,216	0,030	0,102	5,545	0,081	0,074	0,158
47	9 cm 11	0,282	0,038	0,080	3,895	0,042	0,120	0,232
48	10 cm 12	0,473	0,107	0,256	4,412	0,074	0,224	0,288
49	11 cm 12	0,352	0,051	0,189	5,017	0,073	0,165	0,198
50	9,5 cm 12	0,332	0,050	0,132	3,656	0,032	0,065	0,180
51	10 cm 12	0,426	0,073	0,212	6,341	0,042	0,180	0,232
52	10 cm 12	0,489	0,108	0,225	6,191	0,047	0,107	0,062
53	10 cm 13	0,316	0,063	0,143	5,761	0,065	0,077	0,174
54	10 cm 13	0,274	0,037	0,158	5,345	0,057	0,176	0,316
55	2 cm 13	0,329	0,051	0,126	6,223	0,095	0,063	0,171
56	11 cm 14	0,318	0,046	0,127	4,572	0,031	0,125	0,151
57	9 cm 14	0,438	0,072	0,207	6,135	0,094	0,253	0,342
58	9 cm 14	0,536	0,072	0,267	4,157	0,056	0,319	0,391
59	9 cm 14	2,013	0,106	0,163	4,423	0,046	0,307	2,831
60	9,5 cm 15	0,301	0,085	0,081	6,675	0,039	0,082	0,212
61	9,5 cm 15	0,289	0,031	0,093	6,232	0,063	0,082	0,172
62	10 cm 15	0,340	0,052	0,091	5,724	0,068	0,059	0,149
63	10 cm 15	0,456	0,043	0,056	4,698	0,045	0,093	0,201
64	10 cm 15	0,545	0,062	0,081	6,528	0,067	0,126	0,228
65	2 cm 15	0,507	0,055	0,188	4,994	0,039	0,277	0,373
66	10 cm 16	0,610	0,127	0,216	5,013	0,045	0,269	0,329
67	10 cm 16	0,415	0,048	0,117	5,161	0,067	0,086	0,231
68	10 cm 16	0,394	0,103	0,135	6,467	0,089	0,058	0,252
69	11 cm 16	0,508	0,109	0,231	5,005	0,055	0,162	0,328
70	8 cm 16	0,506	0,126	0,239	6,976	0,229	0,201	0,326
71	10 cm 17	0,404	0,047	0,121	4,234	0,067	0,068	0,266
72	11 cm 17	0,397	0,078	0,101	4,308	0,041	0,038	0,194
73	11 cm 17	0,976	0,081	0,165	8,039	0,128	0,245	0,496
74	10 cm 18	0,346	0,090	0,209	4,297	0,074	0,147	0,244
75	10 cm 18	0,460	0,059	0,163	5,233	0,057	0,122	0,253
76	10 cm 18	0,850	0,093	0,161	4,565	0,073	0,135	0,313
77	10 cm 18	0,371	0,068	0,116	6,078	0,065	0,051	0,265
78	8,5 cm 18	0,305	0,084	0,234	6,080	0,071	0,136	0,069
79	10 cm 19	0,393	0,104	0,163	3,651	0,066	0,087	0,104
80	7 cm 19	0,400	0,094	0,244	4,087	0,085	0,290	0,337
81	9 cm 20	0,799	0,158	0,361	4,705	0,075	0,377	0,378
82	9 cm 20	0,798	0,155	0,360	4,714	0,093	0,464	0,436

Table 2 – The first 3 principal components whit eigenvalues above 1 from main correlation.

Component Loadings

	RC 1	RC 2	RC 3	Uniqueness
Ca	.	.	0.893	0.222
Cl	0.950	.	.	0.100
K	0.980	.	.	0.130
Mg	.	.	0.768	0.284
NO3	.	0.899	.	0.246
Na	0.644	0.394	.	0.258
SO4	.	0.861	.	0.159

Table 3 - Pearson Correlation matrix and p-values between the major ions records. In bold the values above r > 0.5. Underlined the correlation values whit p< 0.001. Not in table the correlation values whit r < 0.1.

		NO_3	**SO_4**	**Ca**	**Mg**	**Na**	**K**
Cl	Pearson's	0.147	0.409	-	0.044	**0.654**	**0.840**
	p-value	0.189	< .001	0.496	0.694	< .001	< .001
NO_3	Pearson's	—	**0.557**	0.04	0.324	0.198	-
	p-value	—	< .001	0.714	0.003	0.075	0.829
SO_4	Pearson's		—	-	0.166	**0.667**	0.204
	p-value		—	0.293	0.137	< .001	0.066
Ca	Pearson's			—	0.390	-	-
	p-value			—	< .001	0.297	0.121
Mg	Pearson's				—	0.107	-
	p-value				—	0.337	0.622
Na	Pearson's					—	**0.513**
	p-value					—	< .001